Dalton Transactions

Accepted Manuscript

ROYAL SOCIETY OF CHEMISTRY

www.rsc.org/dalton

Lattice defects and thermoelectric properties: The case of p-type $CuInTe_2$ chalcopyrite by introduction of zinc

Jiangfeng Yang,[a,b] Shaoping Chen,[a]* Zhengliang Du,[b] Xianglian Liu,[b] Jiaolin Cui [b]*

Received (in XXX, XXX) Xth XXXXXXXXX 200X, Accepted Xth XXXXXXXXX 200X
DOI: 10.1039/b000000x

ABSTRACT I-III-VI_2 chalcopyrites have unique inherent crystal structure defects, hence have a potential to be thermoelectric candidates. Here we identified mixed polyanionic/polycationic site defects (Zn_{In}^-, V_{Cu}^-, In_{Cu}^{2+} and/or Zn_{Cu}^+) upon Zn substitutions for either Cu or In or both in $CuInTe_2$, with species Zn_{In}^- originating from the site preference of Zn on the cation 4*b* site. Because of the mutual reactions among these charged defects, Zn substitution in $CuInTe_2$ alters the basic conducting mechanism, and simultaneously changes the lattice structure. The alteration of the lattice structure can be embodied in an increased anion position displacement (u), or reduced bond length difference (Δd) between $d_{(Cu\text{-}Te)4a}$ and $d_{(In\text{-}Te)4b}$ with Zn content increasing. Because of that, the lattice distortion diminishes and the lattice thermal conductivity (κ_L) enhances. However, the material with Zn simultaneous substitutions for Cu and In gives low lattice κ_L, therefore, we attained the highest ZT value of 0.69 at 737K, which is 1.65 times that Zn-free $CuInTe_2$.

1. Introduction

Thermoelectric (TE) technology has a great potential to directly convert waste heat into electricity, hence it has attracted much attention in recent years. However, the relatively low efficiencies of current TE modules limit their large–scale commercialization. At issue is that three physical parameters including Seebeck coefficient (α), electrical conductivity (σ) and thermal conductivity (κ) that govern the TE performance are interrelated, which makes it hard to optimize them simultaneously. In order to improve the TE performance, we need to further explore new materials like chalcopyrites[1] which have inherent low κ and high α values usually. However, their electrical conductivities have to be improved.

$CuInTe_2$ (CIT) is a member of ternary I–III–VI_2 compounds with diamond–like structure (I=Cu, Ag; III=Al, Ga, In; VI=S, Se, Te). Its direct bandgap (E_g) is around 1.02eV.[2] The crystal of $CuInTe_2$ often shows a tetragonal distortion due to $u \neq 0.25$ and $\eta = c/2a \neq 1$ and unequal cation–anion distance $d_{Cu-Te} \neq d_{In-Te}$ (here the u and η are the anion position displacement parameters, and a and c are the lattice parameters).[3] Any occupations of foreign elements in the cation sites of $CuInTe_2$ will cause the redistribution of the bond charges between Cu–Te and In–Te, thus leading to a tiny adjustment of the crystal structure.[4] In addition, upon the occupations of impurity atoms (Me) in the cation sites, the simple conducting mechanisms will become more complicated by the presence of donor–acceptor defect pairs ($2V_{Cu}^- + In_{Cu}^{2+}$)[3,5] and potential creation/annihilation of those in the Me–substituted compounds, thus modifying physical properties. For example, in Mn–substituted $CuGaSe_2$ there are two antisite defects (Mn_{Cu}^+ and Mn_{Ga}^-) created,[6] the Mn_{Cu}^+ of which decreases the concentration of Cu vacancies (V_{Cu}^-), which thereby reduces the p–type carrier concentration. While the effect of p–type Mn_{Ga}^- could neutralize that of inherent Ga_{Cu}^{2+}, so that the material exhibits ferromagnetic behavior.[6] In Mn–substituted $CuInTe_2$, the samples with 3% Mn substitution in Cu sites are paramagnetic, but at higher Mn concentration ($9\% < x < 12\%$), they show antiferromagnetic coupling.[7] Moreover, the site preference of some elements in ternary I–III–VI_2 could form unexpected functional units. For instance, in Mn–substituted $CuInSe_2$ Mn prefers the Cu site[8] or In site under Cu–rich and In–poor conditions,[9] which helps forming the antisite defcet Mn_{Cu}^+ or Mn_{In}^-. The formation of Mn_{Cu}^+ could help to create the electrically conducting unit Mn–Se,[10] thus enhancing the electrical conductivity of $CuInSe_2$.

Since element Zn has an electronegativity of 1.65, smaller than those of In (1.78) or Cu (1.9), we believe that upon the addition of Zn in CIT, Zn occupies the cation (In or Cu) sites, rather than anion (Te) sites. Such occupations favour the formation of slab ZnTe, which reduces the Te *p*–Cu *d* repulsion near the upper valence band (VBM)[11] and cause a splitting of the valence band into two subbands due to band–anticrossing effect (BAC).[12] This effect was also observed when Cu was introduced into As_2Se_3[13] and oxygen into ZnSe.[14,15] In this light, the bandgap narrows due to an appearance of extended states or impurity level into the midgap region, thus increasing the Seebeck coefficient.[15]

In this work, we identified multiple antisite defects (Zn_{In}^-, V_{Cu}^-, In_{Cu}^{2+} and/or Zn_{Cu}^+) via the substitutions of element Zn for either Cu or In or both in the $CuInTe_2$. Such substitutions alter the basic conducting mechanism and lattice structures, tuning the TE performance of $CuInTe_2$.

2. Experimental

Sample preparations Three sorts of compounds $Cu_{1-x}In_{1-x}Zn_{2x}Te_2$ (CI–poor), $CuIn_{1-x}Zn_xTe_2$ (In–poor) and $Cu_{1-x}InZn_xTe_2$ (Cu–poor) (x=0, 0.02, 0.05, 0.1, 0.2) were synthesized in different evacuated silica tubes via high–temperature, solid–state reactions of four elements (Cu, In, Te and Zn) with the purity of 5N at 1373K for 24h in a programmable furnace. The melts were then slowly cooled to 650 ^oC, and dwelled at this temperature for 240h in vacuum. Subsequently, the ingots were cooled in furnace to room temperature (RT). Such a synthesis process assures

near–equilibrium chemical compositions or only a chalcopyrite–type structure to be obtained without phase transtion.[16]

The as–solidified ingots were pulverized and then ball–milled in stainless steel bowls which contain benzinum at a rotation rate of 350 rpm for 5 h. The dried powders were quickly sintered by using spark plasma sintering apparatus (SPS–1030) with a designed sintering program under a pressure of 50 MPa. The densities of the sintered samples were measured by using Archimedes' method. Each sample was cut into 3–mm slices measuring 2.5 mm×12 mm out of the sintered block with a size of ϕ20 mm×2.5 mm for electrical property measurements.

Physical measurements The Seebeck coefficients (α) and electrical conductivity (σ) as a function of temperature were measured by using a ULVAC ZEM–2 instrument system in helium atmosphere from RT to 740K. A temperature difference of around 5 ^{o}C has been applied between two terminals of the sample to measure the Seebeck coefficient, whereas the electrical conductivity was measured by using the 4–probe method. According to several repeated measurements in the same samples, it is evidenced that the data corrected are of good accuracy with the errors of both the Seebeck coefficient and electrical conductivity below 10.0%. The thermal conductivities (κ) at RT~735K were calculated as the products of material densities, thermal diffusivities (with the error below 10.0%) and specific heats (with the error below 6.0%) measured by a laser flash method (TC–1200RH apparatus). The Hall coefficient (R_h) measurements at RT were conducted on a Physical Property Measurement System (PPMS, Model–9) by using a four–probe configuration with a magnetic field sweeping between ±1.0T and then performed on rectangular samples with the size of 2×2×8 cm^3. The Hall mobility (μ) and carrier concentration (n) were subsequently calculated from the relations $\mu = R_h\sigma$ and $n=1/(eR_h)$ respectively, where e is the electron charge. The current and Hall voltage leads were fine copper wires, and the contacts were made of silver paste. The absorption coefficient measurements were carried out by using Perkine–Elmer Lambda 950 UV–VIS–NIR spectrophotometer, and absorption spectra for the powders were recorded between the visible and part of infrared regions (200–900 nm).[17]

Structural analysis The structural analysis of the powders was made by powder x–ray diffractometer (D8 Advance) operating at 50 kV and 40 mA, using Cu Kα radiation (λ=0.15406 nm) and a scan rate of 4° min^{-1} to record the patterns ranging from 10° to 100°. Rietveld refinements using XRPD were performed using FULLPROF, and X–ray diffraction peakshapes were quantified by a Pseudo–Voigt function and a Pseudo–Voigt function with the Finger–Cox–Jephcoat asymmetry correction, respectively. The background was described as a shifted Chebyschev type. In chalcopyrite–type $CuInTe_2$, there are two cation sites, Cu on site 4a (0, 0, 0) and In on site 4b (0, 0, 0.5). The anion Te atoms on site 8d (x_{Te}, 0.25, 0.125 with x_{Te}~0.25) are coordinated by two Cu and two In cations. The following parameters were refined: lattice parameters, peak shape parameters, atomic coordinates, isotropic displacement parameters (U_{iso}) and site occupation factors (SOFs). Each structural model was refined to convergence.

Band structure and formation energy calculations The *ab inito* calculation was performed by using plane–wave pseudopotential technique with CASTEP software [18] based on density functional theory (DFT). The generalized gradient approximation (GGA) [19] was used, and the Perdew, Burke, Ernzerhof (PBE) functional was adopted as the exchange–correlation energy. We used the norm conserving pseudopotential with a cutoff energy of 500eV and a k mesh of 4×4×2 for geometry optimizations. The $3d^{10}4s^1$, $5s^25p^1$, and $5s^25p^4$ were treated as valence states of Cu, In, and Te respectively. In the geometrical optimization, all forces on atoms are converged to less than 0.03eVÅ^{-1}. The maximum ionic displacement is confined within 1×10^{-3}Å and the total stress tensor is reduced to the order of 0.05GPa.

We used four formula units per conventional cell model, which was composed of four Cu, four In and eight Te atoms. The doping conditions are assumed to retain the same structure, but Zn was arranged in Cu, or In or both lattice sites, which corresponds to Zn occupations in the Cu (25.0 at.%) and In (25.0 at.%) lattice sites.

When calculating the formation energies, we have also used generalized gradient approximation (GGA) but with a cutoff energy of 400 eV and a k mesh of 4×4×3.

X–ray photoelectron spectroscopy X–ray photoelectron spectra (XPS) were measured on a AXIS ULTRA DLD equipped with a monochromatic Al Ka X–ray source (30mA, 15 kV) and a hybrid lens. Samples were sputter–cleaned with an Art ion beam until core–line peaks associated with surface oxides were no longer observed in the XPS spectra. High–resolution core–line spectra of Zn2$p_{3/2}$, Cu2$p_{3/2}$, In3$d_{5/2}$, and Te3$p_{5/2}$ were collected. Because of low concentration of Zn in the Cu (In)– and CI–poor compounds, only three Zn–rich members ($Cu_{0.9}In_{0.9}Zn_{0.2}Te_2$, $Cu_{0.9}InZn_{0.1}Te_2$ and $CuIn_{0.9}Zn_{0.1}Te_2$) were examined. $CuInTe_2$ was examined for comparison.

3. Results and discussions

X–ray diffraction patterns for three kinds of samples are shown in Fig.S1. No visible impurity phases were identified at x<0.2. This indicates that almost Zn atoms have been incorporated into the crystal lattice, and the materials crystallize in a single chalcopyrite structure (PDF 34–1498). At x=0.2, a minor ZnTe phase (PDF 19–1482) was indentified in the In(Cu)–poor systems, we therefore stop the investigations of the materials that contain x> 0.2 Zn contents.

The band structure of CIT and its density of states (DOS) are presented in Fig.S2(a,b), where a direct band gap was observed (E_g =1.09eV). The Fermi level (E_F) lies in the valence band maximum (VBM). When Zn atoms (25.0 at.%) occupy Cu and In sites simultaneously, the E_g value gets small (E_g=0.75eV), and a relatively flat band was observed near the E_F compared to CIT (see Fig.S2c,d), suggesting that there is a potential increase in the effective mass of the valence band. When Zn atoms (25.0 at.%) settle in the Cu sites only, E_F moves to the conduction band with E_g=0.95eV, as shown in Fig.S3(a,b), suggesting that material exhibits n–type conduction. However, E_F drops to the valence band with E_g=0.30eV as Zn settles in In sites (25.0 at.%) (Fig.S3c,d). Such a significant reduction of the bandgap E_g upon Zn occupation in In sites seems to be caused by the impurity level of ZnTe just above the VBM (red line In Fig.S3c) that enters the midgap region.[12,15] However, we did not observe the so–called impurity–induced peak in the density of states (DOS) caused by the BAC effect,[12] even though there is a relatively high DOS near the Fermi level, as shown in Fig.S3d.

Above calculations reveal that the different occupations of Zn have different effects on band structures. However, in the actual materials upon Zn substitutions we have only observed a little widening tendency of the bandgap compared to Zn–free CIT. The E_g value remains almost unchanged (0.8~0.85eV) in three Zn–substituted materials, regardless of the Zn content (see Fig.S4a–c). This implies that in the actual materials the creation of the defects due to an introduction of Zn is not so simple as what we anticipated. There must be multiple antsite defects, each of which plays its own role.

In order to determine the exact locations of Zn and antisite defects in Zn–substituted CIT in the real materials, we have calculated the formation energies when Zn occupies either Cu or In or both sites based on the following reactions:

$Cu_4In_4Te_8+Zn=Cu_4In_3ZnTe_8+In$ (Occupying In lattice sites) (1)

$Cu_4In_4Te_8+Zn=Cu_3ZnIn_4Te_8+Cu$ (Occupying Cu lattice sites) (2)

$Cu_4In_4Te_8+2Zn=Cu_3In_3Zn_2Te_8+Cu+In$ (Occupying both Cu and In lattice sites) (3)

Then, we attain:

$E_f=E_f(Cu_4In_3ZnTe_8)+E_T(In)-E_T(Cu_4In_4Te_8)-E_T(Zn)$ (4)

$E_f=E_f(Cu_3ZnIn_4Te_8)+E_T(Cu)-E_T(Cu_4In_4Te_8)-E_T(Zn)$ (5)

$E_f=E_f(Cu_3In_3Zn_2Te_8)+E_T(Cu)+E_T(In)-E_T(Cu_4In_4Te_8)-2E_T(Zn)$ (6)

Where E_f is the formation energy and E_T is the total energy of each material.

The results reveal that the formation energies (E_f) are –5.943eV, –4.549eV and –2.184eV, respectively, which corresponds to the Zn occupation in the In, Cu and both lattice sites. This suggests that Zn has a site preference on In rather than on Cu sites, and the simultaneous occupations of Zn in Cu and In sites have least possibilities.

To further confirm the site preferences of Zn, we have calculated the SOFs for CI–poor, Cu(In)–poor systems using Rietveld refinement, according to the two models proposed below:

Model A: $(Cu, In, Zn)_{4a}(In, Cu, Zn)_{4b}(Te_{2-\delta})_{8d}$

Model B: $(In, Zn)_{4a}(In, Cu, Zn)_{4b}(Te_{2-\delta})_{8d}$

In model A, the cation sites (4*a* and 4*b*) are proposed to be occupied by Cu, Zn, and In ions simultaneously, while in model B the 4*a* sites are only occupied by In and Zn ions, that is,

for model A,

$SOF(Cu)_{4a}+SOF(Zn)_{4a}+SOF(In)_{4a}=1$ (7)

$SOF(Cu)_{4b}+SOF(Zn)_{4b}+SOF(In)_{4b}=1$ (8)

$SOF(Zn)_{4a}+SOF(Zn)_{4b}=0.02,\ 0.05$ and 0.1 (9)

for model B,

$SOF(In)_{4a}+SOF(Zn)_{4a}=1$ (10)

$SOF(Cu)_{4b}+SOF(Zn)_{4b}+SOF(In)_{4b}=1$ (11)

$SOF(Zn)_{4a}+SOF(Zn)_{4b}=0.02,\ 0.05$ and 0.1 (12)

The final results using model B for the sample at x=0.1 are shown in Table I. The preliminary fitting results are presented in Table SI–III and Fig.S5. We observed that Zn has a site preference on In rather than on Cu sites in three materials, which is in accordance with those obtained by energy formation calculation. Besides, Cu has little possibility to occupy In sites, and indium has an increasing tendency to occupy the Cu sites as Zn content increases, which is specified in model B.

Because of the site preference of Zn, the materials create a large quantity of site defect Zn_{In}^-. However, we can not rule out the defects Zn_{Cu}^+ and In_{Cu}^{2+} as donors originated from the occupations of Zn and expelled In ions in the Cu sites. Such creations of defects could reduce the inherent Cu vacancies (V_{Cu}^-) in CIT, and disturbs the original Coulomb attraction between In_{Cu}^{2+} and $2V_{Cu}^-$.[20] As a consequence, there must be mixed polyanionic/polycationic species in Zn–substituted CIT, with each making its own contributions.

In order to confirm the existence of the species (Zn_{In}^-, Zn_{Cu}^+ and In_{Cu}^{2+}), we need to determine the oxidation states of Cu, Zn and In using XPS spectra of Cu2*p*, Zn2*p* and In3*d*, the results are shown in Fig.1. The average binding energy (BE) values with uncertainties estimated at ~±0.01 eV are listed in Table II, where we observed that the BE values of Zn2$p_{3/2}$ (1021.8~1022.0eV) are all higher than that of single element Zn (1021.45eV), but very close to that of ZnTe.[21] We therefore confirm the existence of ionic Zn^{2+}. On the other hand, the absence of a satellite (at 940–945 eV) above the 2$p_{3/2}$ core–line peak in the Cu2*p* spectra (see Fig.1) and resemblance of Cu2*p* spectra to the reported in *ref*. [10] and copper (I) halides (e.g. CuBr, CuI) [22] can confirm the presence of Cu^+. In addition, the In 3$d_{5/2}$ BE (444.6 eV) in three materials is higher than that of elemental In (443.8eV), but almost equals to those in In_2O_3 (444.7eV) and In_2Se_3 (444.6 eV),[21] which indicates the presence of positively charged In^{3+} species. Therefore, the antisite defects Zn_{Cu}^+ and Zn_{In}^- can be confirmed upon Zn settling in the Cu or In sites. The formation of In_{Cu}^{2+} is attributed to the occupation of expelled In ions in the Cu sites, as mentioned above. The schematic model of a cell upon creations of these defects in $CuInTe_2$ chalcopyrite is shown in Fig.S6.

The creation of the defect Zn_{In}^- (Zn_{Cu}^+) drops (moves) E_F into the acceptor (donor) level, which might narrow (widens) the bandgap (see Fig.S3), while the reduction[4(b)] or creation[23] of V_{Cu}^- could conserve or increase the bandgap in Cu–Ga(In)–Te(Se)$_2$ systems. That is why we did not observe a visible change of the bandgap in three sort of materials. On the other hand, the response of each species to the carrier concentration n is also different. Some species acts as donors, while the others as acceptors. The detailed responses are estimated and summarized in Table III. Taken together, the p–type carrier concentration (n) in CI–poor system has an increasing tendency, while those in In– and Cu–poor systems show a decreasing tendency. In order to verify these estimations, we have measured Hall coefficients (R_h) and carrier concentrations (n) at RT, and found that the n value in CI–poor system enhances from 7.74×10^{25} (x=0.02) to 9.65×10^{25} (m^{-3}) (x=0.1), which is more than one order of magnitude higher than that in Zn–free CIT ($2.65\times10^{24}m^{-3}$).[1(d)] While the n value in In (Cu)–poor system decreases from 2.86 (11.90)$\times10^{24}$ (x=0.02) to 2.33(7.79)$\times10^{24}$ (m^{-3}) (x=0.1) (see Table IV), thus clearly confirming the above estimations shown in Table III. However, the carrier concentrations in In– or Cu–poor system are about one to two orders of magnitude smaller than the optimal one (10^{25} to 10^{26} m^{-3}),[24] which implies that there is still a big room for the improvement of TE performance.

The TE properties of CI–poor system are presented in Fig.2, where we observed that the Seebeck coefficients (α) at x>0.02 increases with temperature over all the measuring temperature range, but gradually decreases with Zn content increasing (Fig.2a). Although the α values are lower than those of CIT when T<670K, they gradually approach at T > 700K. The maximum α value (x=0.02) is 212.0 (μV/K) at 737K. The electrical conductivity (σ) upon Zn addition, which is much higher than those of Zn–free CIT, decreases with temperature (Fig.2b). At 737K the σ value (x=0.02) is 2.16×10^4 ($\Omega^{-1}m^{-1}$), increasing by about a factor of 1.5 compared to Zn–free CIT. In addition, the CI–poor system gives much lower κ_L values (~0.65 w$\kappa^{-1}m^{-1}$) when x<0.05 at 737K, however, it shows an increasing tendency with Zn content increasing above 650K . At x=0.1 the κ_L value reaches ~3.05 w$\kappa^{-1}m^{-1}$ at 737K (Fig.2c), an insert in Fig.2c is the relation of total $\kappa(T)$ that presents almost the same temperature dependence as κ_L. Combining the three parameters we have attained the highest ZT value 0.69 at 737K at x=0.02 (Fig.2d), increasing by a factor of 1.65 compared to Zn–free CIT. The ZT value is much higher than those of $CuInTe_2$ (ZT=0.27~0.5 at 600~710K)[1(d-f)] and $Zn_{0.03}Cu_{0.97}FeS_2$ (ZT=0.04 at 400K)[25], and it can be comparable to that of $Ag_{0.95}GaTe_2$ (ZT=0.77 at 850K).[1(c)] However, it is much lower than that of $CuGaTe_2$[1(a)] (ZT=1.45 at 940K) and reported $CuInTe_2$ (ZT=1.18 at 850K).[1(b)]

In In (Cu)–poor systems, the temperature dependences of both α and σ are also quite different from those of CIT, as shown in Fig.3(4)a,b. However, these two sorts of materials exhibits similar temperature dependence of the Seebeck coefficient, so do their α values for each Zn content. The reason is that the effective masses m^* and carrier concentration (n) optimize, according to the relation: $\alpha = \frac{8\pi^2 K_B^2 T}{3eh^2} m_d^* \left(\frac{\pi}{3n}\right)^{\frac{2}{3}}$,[26] as shown in Table IV. In addition, the σ value increases with Zn content increasing in both systems. Relatively high electrical conductivities in In (Cu)–poor systems might be that the widening of the bandgap prevents the minority carriers from thermally activation at high temperatures,[27] rather than due to the introduction of the impurity level that narrows the bandgap and then facilitates the thermal activation of electrons from the conduction band.[28] Moreover, two sorts of materials give high lattice κ_L values compared to CI–poor counterparts, which show increasing tendency with Zn content increasing above ~550K (an insert is the relation of total $\kappa(T)$), see Fig.3(4)c. Therefore, we can only attain limited ZT values (0.34 (0.43) at x=0.02 to 0.20 (0.21) at x=0.1) in these two systems (Fig.3(4) d).

Although three sorts of materials reveal similar Zn content dependences of electrical properties, the Zn substitution in CIT alters the basic conducting mechanism in that these materials give different carrier concentrations and mobility (see Table III and IV). In CI–poor samples, the p–type carrier concentrations are high as they form a large quantity of antisite defect Zn_{In}^- and copper vacancy V_{Cu}^- as acceptors, even though there are small quantities of Zn_{Cu}^+ and In_{Cu}^{2+} which tends to cancel the p–type carriers to some degree. In this regard, the negative effect of the increased n value on the Seebeck coefficient seems to be cancelled by the large effective masses m^* (m^*=1.03~1.09) in CI–poor samples. However, in In–poor samples the situation has changed. In spite of the fact that the carrier concentrations are not high due to an increased donor defect In_{Cu}^{2+} and limited p–type copper vacancy V_{Cu}^-, but the effective masses m^* are low compared to those in the CI–poor counterparts, hence the α values can still be comparable to those in the CI–poor samples (Fig.3a). In Cu–poor samples they have large quantities of Zn_{In}^- and V_{Cu}^- as acceptors due to Cu deficiency, but there are a certain amount of Zn_{Cu}^+ and significantly increased In_{Cu}^{2+}. Therefore, the total carrier concentration n in Cu–poor samples reveals a decreasing tendency (Table IV). Because the effective masses m^* (0.32 at x=0.02 to 0.17 at x=0.1) are not high, hence the Cu–poor systems do not give much high α values yet (Fig.4a). Likewise, the electrical conductivity bears little relation to the chemical compositions either (Fig.3,4a,b), because the σ values are governed by two competing parameters n and μ simultaneously (Table IV).

In the present CIT and its based chalcopyrites, the bond lengths between cation–anion are determined to be 0.26~0.28nm using Rietveld refinements, which is comparable to the size of the mean free path of the phonons in solids (~0.3 nm).[29] In this light, any tiny adjustment of the crystal distortion will alter the phonon scattering mechanism, changing the lattice part (κ_L) at high temperatures.[4] On the other hand, the parameters u (η), representing the anion position displacement in the chalcopyrites,[3(b),30] show an increasing (decreasing) tendency with the Zn content increasing, and all approaches the equilibrium values (u=0.25, η=1)[3(b)] (Table IV). This suggests that the lattice distortion gets diminished, which accounts for the enhancement of κ_L. To further confirm this issue, we have calculated the bond lengths of $d_{(Cu–Te)4a}$ and $d_{(In–Te)4b}$ values through Rietveld refinements using the parameters shown in Table 1. The results are shown in Fig.5, where we observed that the $d_{(Cu–Te)4a}$ exhibits an linear tendency of increasing, while the $d_{(In–Te)4b}$ shows a decreasing tendency with Zn content increasing. These results clearly reveal that the bond length differences (Δd) between Cu–Te and In–Te is gradually reduced, thus clarifying the diminution of the lattice distortion.

On the other hand, the lattice part κ_L has a direct correlation with the phonon relaxation time τ which mainly consists of point defects (τ_D), phase/grain boundaries (τ_B), Umklapp (τ_U) and normal processes (τ_N),[31] Which is:

$$\tau^{-1} = \tau_D^{-1} + \tau_B^{-1} + \tau_U^{-1} + \tau_N^{-1} \quad (13)$$

However, we only need to concentrate on the point defects (τ_D) in the present material systems in that three sorts of materials give similar τ_B, τ_U and τ_N. In CI–poor system there are increased p–type defects upon Zn substitutions, which thereby tends to reduce τ_D and κ_L value significantly at high temperatures. While in the Cu(In)–poor systems the p–type carriers all show decreasing tendency, therefore, the τ_D values tend to be increased. That is why we have observed the relatively high κ_L

4. Conclusions

Upon different Zn settling in $CuInTe_2$ we observed multiple polyanionic/polycationic antisite defects (Zn_{In}^-, V_{Cu}^-, In_{Cu}^{2+} and/or Zn_{Cu}^+), each of which makes its own contribution to the band structure and transport properties. In general, the Zn substitution in $CuInTe_2$ alters the basic conducting mechanism, but both the Seebeck coefficient and electrical conductivity bear little relation on the Zn content. The lattice thermal conductivity (κ_L) enhances with Zn content increasing due to diminished lattice distortion, which is confirmed by the reduced difference of the bond length (Δd) between $d_{(Cu–Te)4a}$ and $d_{(In–Te)4b}$ and gradually increased anion position displacement u. However, the CI–poor sample (x=0.02) gives a higher lattice distortion and lower κ_L compared to Cu(In)–poor counterparts, so that we have attained the highest ZT value (0.69 at 737K), which is increased by a factor of 1.65 compared to Zn–free CIT.

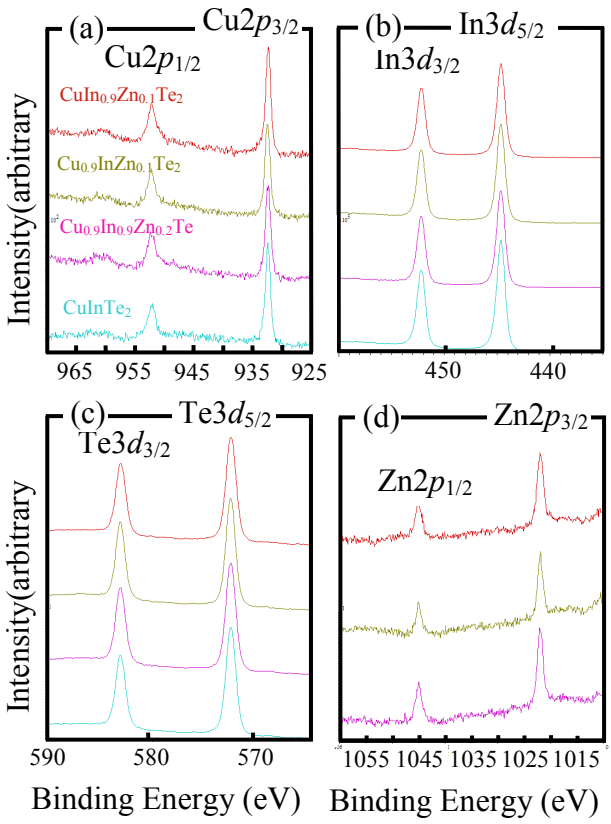

Fig.1 XPS spectra of (a) Cu2*p*, (b) In3*d*, (c) Te3*d* , and (d) Zn2*p* for $CuInTe_2$, $Cu_{0.9}In_{0.9}Zn_{0.2}Te_2$, $Cu_{0.9}InZn_{0.1}Te_2$, and $CuIn_{0.9}Zn_{0.1}Te_2$.

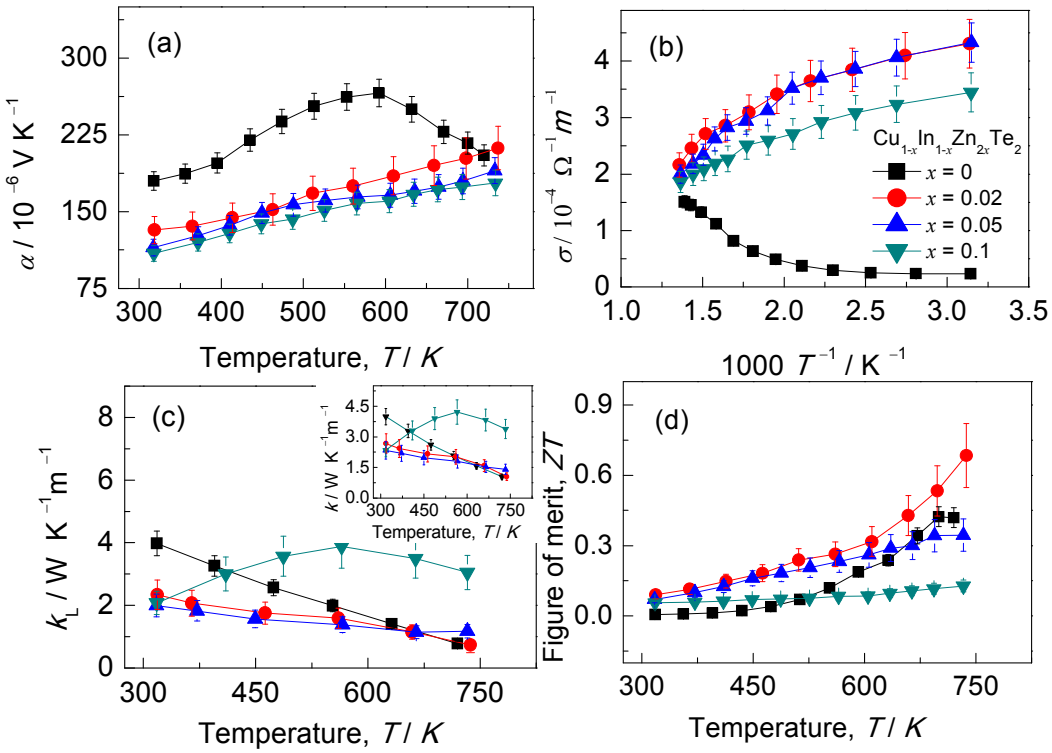

Fig.2 Thermoelectric properties of $Cu_{1-x}In_{1-x}Zn_{2x}Te_2$, (a) Seebeck coefficients (α), (b) electrical conductivities (σ), (c) lattice thermal conductivities (κ_L), an insert is the relation κ–T, (d) ZT values.

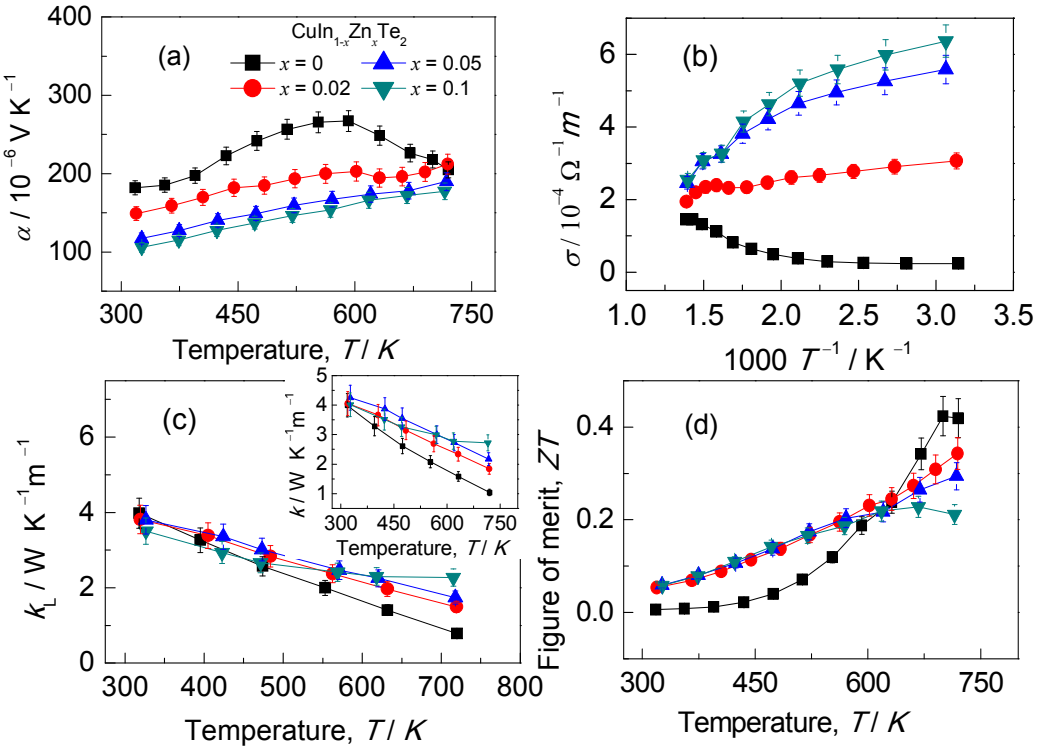

Fig.3 Thermoelectric properties of $CuIn_{1-x}Zn_xTe_2$, (a) Seebeck coefficients (α), (b) electrical conductivities (σ), (c) lattice thermal conductivities (κ_L), an insert is the relation κ–T, (d) ZT values.

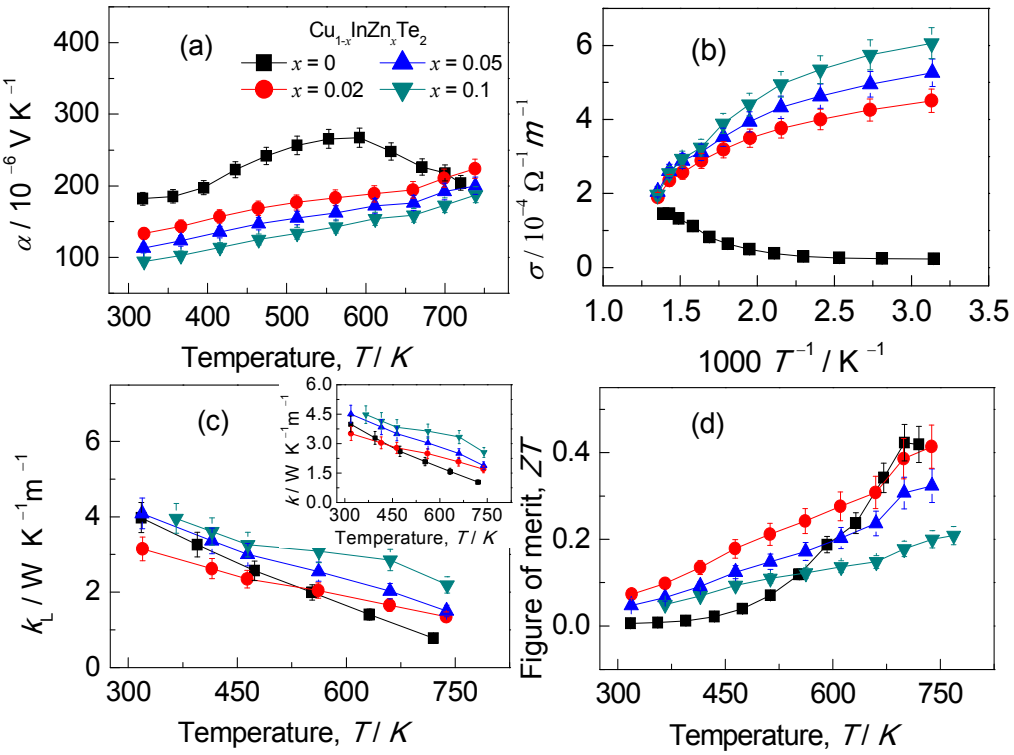

Fig.4 Thermoelectric properties of $Cu_{1-x}InZn_xTe_2$, (a) Seebeck coefficients (α), (b) electrical conductivities (σ), (c) lattice thermal conductivities (κ_L), an insert is the relation κ–T, (d) ZT values.

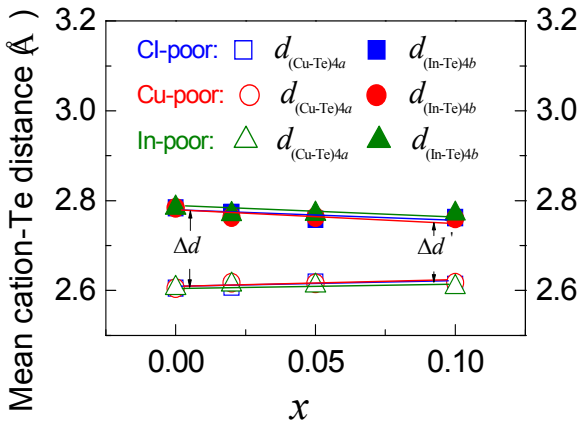

Fig.5 Zn content (x) versus mean cation–Te distance derived from Rietveld refinements using X-ray powder diffraction experiment.

Table I Structural parameters and refinement details for CI–poor, Cu–poor and In–poor compounds (x=0.1) obtained by Rietveld refinements

Parameters	CI–poor	Cu–poor	In–poor
	Model B	Model B	Model B
	Cation 4*a*		
SOF(Cu)	0.9000	0.9000	1.0000
SOF(In)	0.1297	0.1615	0.0891
SOF(Zn)	0.0297	–0.0615	0.0891
100Uiso (Å ^{2})	1.0950	1.4010	1.1720
	Cation 4*b*		
SOF(In)	0.8448	0.9090	0.8997
SOF(Cu)	0.0000	0.0000	0.0000
SOF(Zn)	0.1552	0.0910	0.1003
100Uiso (Å ^{2})	2.0490	1.5530	2.3910
	Anion 8*d*		
SOF(Te)	1.0044	0.9929	0.9997
100Uiso (Å ^{2})	2.1460	1.9780	2.1100
x_{Te}	0.2312	0.2299	0.2269
	Reliability factors		
χ^2	1.570	1.6290	1.9870
WRp	0.0883	0.0887	0.0999
Rp	0.0681	0.0688	0.0767

Table II Binding energies of Zn2$p_{3/2}$, Cu2$p_{3/2}$, In3$d_{5/2}$, and Te3$d_{5/2}$ core-level photoelectron spectra for $CuInTe_2$, $Cu_{0.9}In_{0.9}Zn_{0.2}Te_2$, $Cu_{0.9}InZn_{0.1}Te_2$ and $CuIn_{0.9}Zn_{0.1}Te_2$ compounds

Compounds	Zn2$p_{3/2}$ (eV)	Cu2$p_{3/2}$ (eV)	In3$d_{5/2}$ (eV)	Te3$d_{5/2}$ (eV)
$CuInTe_2$		932.5	444.6	572.6
$Cu_{0.9}In_{0.9}Zn_{0.2}Te_2$	1022.0	932.4	444.6	572.6
$Cu_{0.9}InZn_{0.1}Te_2$	1021.8	932.6	444.6	572.7
$CuIn_{0.9}Zn_{0.1}Te_2$	1021.9	932.4	444.6	572.6

Table III Formations of cations (anions) and estimated changes of the carrier concentration (n) in different Zn–substituted $CuInTe_2$

Possible formations of defects	Conducting type	Estimated carrier concentration (n)	Estimated change in n with x
$Cu_{1-x}In_{1-x}Zn_{2x}Te_2$ (CI–poor)			
Zn_{In}^{-}	acceptor	A large quantity	Increase with x increasing
V_{Cu}^{-}	acceptor	A relatively large quantity	Increase with x increasing
Zn_{Cu}^{+}	donor	A small quantity	No significant change
In_{Cu}^{2+}	donor	A small quantity	Increase with x increasing
Taken together, p–type carrier concentration (n) in CI–poor			Increasing tendency
$CuIn_{1-x}Zn_xTe_2$ (In–poor)			
Zn_{In}^{-}	acceptor	A large quantity	Increase with x increasing
V_{Cu}^{-}	acceptor	A limited quantity	Decrease with x increasing
Zn_{Cu}^{+}	donor	/	/
In_{Cu}^{2+}	donor	A small quantity	Increase with x increasing
Taken together, p–type carrier concentration (n) in In–poor			Decreasing tendency
$Cu_{1-x}InZn_xTe_2$ (Cu–poor)			
Zn_{In}^{-}	acceptor	A large quantity	increase with x increasing
V_{Cu}^{-}	acceptor	A large quantity	Relative increase with x increasing
Zn_{Cu}^{+}	donor	A certain quantity	Increase with x increasing
In_{Cu}^{2+}	donor	A small quantity	Significant increase with x increasing
Taken together, p–type carrier concentration (n) in Cu–poor			Decreasing tendency

Table IV Solid state parameters of the solid solutions $CuInTe_2$ based compounds measured at RT

Samples	Hall coefficient, R_h, (m^3C^{-1})	Carrier concentration, n, ($1/m^3$)	Mobility, μ,($m^2\ V^{-1}\ s^{-1}$)	Electrical conductivity, σ, ($W^{-1}\ m^{-1}$)	Seebeck coefficients, α ($\mu V\ K^{-1}$)	Effective mass, m^*	u	η
			$CuInTe_2$ (CIT)					
	2.36×10^{-6}	2.65×10^{24}	5.48×10^{-3}	2.32×10^{3}	181.98	0.16	0.2482	1.0035
			$Cu_{1-x}In_{1-x}Zn_{2x}Te_2$ (CI–poor)					
x=0.02	8.08×10^{-8}	7.74×10^{25}	3.64×10^{-3}	4.32×10^{4}	129.03	1.09	0.2482	1.0036
x=0.05			N/A				0.2484	1.0031
x=0.1	6.48×10^{-8}	9.65×10^{25}	2.27×10^{-3}	3.48×10^{4}	105.34	1.03	0.2485	1.0029
			$CuIn_{1-x}Zn_xTe_2$ (In–poor)					
x=0.02	2.19×10^{-6}	2.86×10^{24}	6.90×10^{-2}	3.09×10^{4}	145.12	0.13	0.2482	1.0035
x=0.05			N/A				0.2483	1.0033
x=0.1	2.68×10^{-6}	2.33×10^{24}	1.76×10^{-1}	6.41×10^{4}	105.23	0.09	0.2485	1.0030
			$Cu_{1-x}InZn_xTe_2$ (Cu–poor)					
x=0.02	5.24×10^{-7}	1.19×10^{25}	2.37×10^{-2}	4.54×10^{4}	131.72	0.32	0.2481	1.0037
x=0.05			N/A				0.2483	1.0035
x=0.1	8.03×10^{-7}	7.79×10^{24}	4.93×10^{-2}	6.13×10^{4}	92.53	0.17	0.2483	1.0034

Acknowledgements

This work is supported by the National Natural Science Foundation of China (51171084, 50871056), Zhejiang Provincial Natural Science Foundation (LY14E010003), Ningbo International cooperation Project (2011D10012), Ningbo Natural Science foundation (2014A610016). We should also acknowledge the band structure calculation from Dr. W.H. Fan in Taiyuan University of Technology, Taiyuan, China

Notes and references

[a] Materials Science and Engineering College, Taiyuan University of Technology, Taiyuan 030024, China

[b] Institute of Materials Engineering, School of Materials, Ningbo University of Technology, Ningbo 315016, China.

* Corresponding author, J.L.Cui, E-mail: cuijiaolin@163.com

Electronic Supplementary Information (ESI) available: [Supporting Information is available from the RSC Online Library or from the author.]. See DOI: 10.1039/b000000x/

REFERENCES

1. (a) T. Plirdpring, K. Kurosaki, A. Kosuga, T.Day, S. Firdosy, V.Ravi, G.J. Snyder, A. Harnwunggmoung, T.Sugahara, Y.Ohishi, H.Mut and S.Yamanaka, *Adv. Mater*., 2012, **24**, 3622; (b) R.L. Liu, H.L. Xi, H.L. Liu, X. Shi, W.Q.Zhang and L.D. Chen, *Chem.Commun*., 2012, **48**, 3818; (c) A.Yusufu, K.Kurosaki, A.Kosuga, T.Sugahara, Y.Ohishi, H.Muta and S.Yamanaka, *Appl. Phys. Lett.*, 2011, **99**, 061902; (d) A.Kosuga, T.Plirdpring, R.Higashine, M.Matsuzawa, K.Kurosaki and S.Yamanaka, *Appl. Phys. Lett*. 2012, **100**, 042108; (e) Y.P.Li, Q.S. Meng, Y. Deng, H. Zhou, Y.L. Gao, Y.Y.Li, J.F. Yang and J.L. Cui, *Appl. Phys. Lett*. 2012,**100**, 231903; (f) N. Cheng, R. Liu, S. Bai, X. Shi and L. Chen, *J. Appl. Phys*. 2014, **115**, 163705.
2. (a) P.Prabukanthan and R.Dhanasekaran, *Mater. Res. Bull*. 2008, **43**, 1996; (b) I. V.Bodnar, A.Eifler, T.Doering, W.Schmitz, K. Bente, V. F.Gremenok, I. A.Victorov and V.Riede, *Cryst. Res. Technol*. 2000, **35**, 1135; (c) M. J.Thwaites, R. D.Tomlinson and M. J.Hampshire, *Inst. Phys. Conf. Ser*. 1997, **35**, 237.
3. (a) J. E.Jaffe and Zunger, A. P*hys. Rev. B* 1983, **29**, 5822; (b) J. E. Jaffe and A. Zunger, *Phys. Rev. B* 1984, **29**, 1882; (c) J. Zhang , R. Liu , N. Cheng , Y. Zhang , J. Yang , C. Uher , X. Shi , L. Chen and W. Zhang, *Adv. Mater.* 2014, **26**, 3848.
4. (a) W.C.Wu, Y.P.Li, Z.L. Du, Q.S.Meng, Z.Sun, W.Ren and J.L.Cui, *Appl. Phys. Lett*. 2013,**103**, 011905; (b) J.L.Cui, Y.P.Li, Z.L.Du, Q.S.Meng and H.Zhou, *J. Mater. Chem. A*, 2013, **1**, 677.
5. S. B.Zhang, S. H.Wei and A. Zunger, *Phys. Rev. Lett*. 1997, **78**, 4059.
6. Y. J. Zhao, A. J. Freeman, *J. Magn. Magn. Mater*. 2002, **246**, 145.
7. L.J. Lin, J. H.Wernick, N.Tabatabaie, G. W.Hull and B. Meagher, *Appl. Phys. Lett*. 1987, **51**, 2051.
8. J.L.Yao, Z.X.Wang, J.V. Tol, N.S.Dalal and J. A. Aitken, *Chem. Mater*. 2010, **22**, 1647.
9. Y. J. Zhao and A. Zunger, *Phys. Rev. B* 2004, **69**, 075208.
10. J.L.Yao, N. J.Takas, M. L.Schliefert, D. S.Paprocki, P. E. R.Blanchard, H.Y.Gou and A.Mar, *Phys. Rev. B* 2011, **84**, 075203.
11. S. B.Zhang, S. H.Wei and A. Zunger, *Phys. Rev. B* 1998, **57**, 9642.
12. W.Shan, W.Walukiewicz, J. W.Ager III and E. E. Haller, *Phys. Rev. Lett*. 1999, **82**, 1221.
13. K.S.Liang, A.Bienenstock and C.W. Bates, *Phys. Rev. B* 1974, **10**, 1528.
14. W.Shan, W.Walukiewicz, J. W.Ager III, K.M.Yu, J.Wu, E.E.Haller, Y.Nabetani, T.Mukawa, Y.Ito and T. Matsumoto, *Appl. Phys. Lett*. 2003, **83**, 299.
15. J.H.Lee, J.Q.Wu and J. C. Grossman, *Phys. Rev. Lett*. 2010, **104**, 016602.
16. L.Roussak, G.Wagner, S.Schorr and K. *J*.Bente, *Solid State Chem*. 2005,**17**, 3476.
17. T. Colakoğlu and M. Parlak *Appl. Surf. Sci*. 2008, **254**, 1569.
18. M.D.Segall, P.J.D.Lindan, M.J.Probert, C.J.Pickard, P.J.Hasnip, S.J.Clark and M.C.Payne, *J. Phys: Condens. Mat*. 2002, **14**, 2717.
19. J.P.Perdew, K.Burke, M. Ernzerhof, *Phys. Rev. Lett*. 1996, **77**, 3865.
20. S.H.Wei, S. B.Zhang and A. Zunger, *Appl. Phys. Lett*. 1998, **72**, 3199.
21. J.F.Moulder and J. Chastain, *Handbook of X-ray Photoelectron Spectroscopy: A Reference Book of Standard Spectra for Identification and Interpretation of XPS Data*; Perkin–Elmer Corporation: Physical Electronics Division, Eden Prairie, Minnesota, p. 261.1992.
22. (a) R. P.Vasquez, *Surf. Sci. Spectra* 1993, **2**, 144; (b) R. P.Vasquez, *Surf. Sci. Spectra* 1993, **2**, 149.
23. S.M.Wasim, C.Rincón, G.Marín and J.M. Delgado, *Appl. Phys. Lett*. 2000, **77**, 94.
24. G. J.Snyder and E. S.Toberer, *Nat. Mater*. 2008, **7**, 105.
25. N.Tsujii and T. Mori, *Appl. Phys. Express* 2013, **6**, 043001.
26. E. S.Toberer, A. F.May and G. J.Snyder, *Chem. Mater*. 2010, **22**, 624.
27. (a) Y.Pei, H.Wang and G. J. Snyder, *Adv. Mater*. 2012, **24**, 6125; (b) A. F. Ioffe, *Semiconductor Thermoelements, and Thermoelectric, Cooling*; Infosearch: London 1957; (c) Y.Pei, A. D.LaLonde, N. A.Heinz, X.Shi, S.Iwanaga, H.Wang, L.Chen and

G. J.Snyder, *Adv. Mater*. 2011, **23**, 5674; (d) A. J.Crocker and L. M. Rogers, *J. Phys. Colloq*. 1968, **29**, C4 129; (e) L. M.Rogers and A. J.Crocker, *J. Phys. D: Appl. Phys*. 1971, **4**, 1016; (f) A. J.Crocker and B. J. Sealy, *J. Phys. Chem*. *Solids* 1972, **33**, 2183; (g) L.Rogers and A. Crocker, *J. Phys. D: Appl. Phys*. 1972, **5**, 1671.

28. (a) J.L.Cui, X.J.Zhang, Y.Deng, H.Fu, Y.M.Yan, Y.L.Gao and Y.Y.Li, *Scripta Mater*. 2011, **64**,510; (b) J. L.Cui, X.L.Liu, X.J.Zhang, Y.Y.Li and Y. Deng, *J. Appl. Phys*. 2011, **110**, 023708.
29. Berman, R. *Thermal Conduction in Solids*; Clarendon Press: Oxford University, 1976.
30. (a) S.C.Abrahams and J.L. Bernstein, *J. Chem. Phys*. 1973, **59**, 5415; (b) S.C.Abrahams and J.L. Bernstein, *J. Chem. Phys*. 1974, **61**, 1140.
31. (a) Y.Luo, J.Yang, G.Li, M.Liu, Y.Xiao; L.Fu, W.Li, P.Zhu, J.Peng, S.Gao and J.Zhang, *Adv. Energy Mater*. 2014, **4**, 1300599; (b) M.Liu and X.Y.Qin, *Appl. Phys. Lett*. 2012, **101**, 132103; (c) M.Liu, X. Y.Qin, C. S.Liu and Z.Zeng, *Appl. Phys. Lett*. 2011, **99**, 062112; (d) H. Y.Lv, H. J.Liu, X. J.Tan, L.Pan, Y. W.Wen, J.Shi and X. F.Tang, *Nanoscale*, 2012, **4**, 511; (e) J.He, S. N.Girard, M. G.Kanatzidis and V.P.Dravid, *Adv. Funct. Mater.* 2010, **20**, 764.

Table of Contents (TOC)

Multiple defects identified in Zn-substituted $CuInTe_2$ are responsible for the reduced difference between $d_{(In–Te)4b}$ and $d_{(Cu–Te)4a}$, improvement of thermoelectric performance.